

Article

Decarbonization of Blast Furnace Gases Using a Packed Bed of Ca-Cu Solids in a New TRL7 Pilot

Jose Ramon Fernandez ^{1,*}, Monica Alonso ¹, Alberto Mendez ¹, Miriam Diaz ¹, Roberto Garcia ¹,
Marcos Cano ², Irene Alzueta ² and Juan Carlos Abanades ¹

¹ CSIC-INCAR, Francisco Pintado Fe, 26, 33011 Oviedo, Spain; mac@incar.csic.es (M.A.); a.mendez@incar.csic.es (A.M.); miriamdg@incar.csic.es (M.D.); roberto.garcia@incar.csic.es (R.G.); abanades@incar.csic.es (J.C.A.)

² Arcelor Mittal R&D Centre, Marqués de Suanes S/N, 33400 Avilés, Spain; marcos.canobertiz@arcelormittal.com (M.C.); irene.alzueta@arcelormittal.com (I.A.)

* Correspondence: jramon@incar.csic.es

Abstract: This work outlines the commissioning and initial experiments from a new pilot plant at Arcelor Mittal Gas Lab (Asturias, Spain) designed to decarbonize up to 300 Nm³/h of blast furnace gas (BFG). This investigation intends to demonstrate for the first time at TRL7 the calcium-assisted steel-mill off-gas hydrogen (CASOH) process to decarbonize blast furnace gases. The CASOH process is carried out in packed-bed reactors operating through three main reaction stages: (1) H₂ production via the water–gas shift (WGS) of the CO present in the BFG assisted by the simultaneous carbonation of CaO; (2) oxidation of the Cu-based catalyst with air, and (3) reduction of CuO with a fuel gas to regenerate CaO and produce a concentrated CO₂ stream. The first experimental campaign used 200 kg of commercial Ca- and Cu-based solids mixed to create a 1 m reactive bed, which is sufficient to validate operations and confirm the process’s effectiveness. A product gas with 40% of H₂ is obtained with CO₂ capture efficiency above 95%. Demonstrating at TRL7 the ability to convert BFG into H₂-enriched gas with minimal CO/CO₂ enables remarkable decarbonization in steel production while utilizing existing blast furnaces, eliminating the need for less commercially developed production processes.

Keywords: CO₂ capture; calcium looping; chemical looping; BFG decarbonization; CASOH



Academic Editor: Giorgio Vilardi

Received: 10 January 2025

Revised: 26 January 2025

Accepted: 29 January 2025

Published: 31 January 2025

Citation: Fernandez, J.R.; Alonso, M.; Mendez, A.; Diaz, M.; Garcia, R.; Cano, M.; Alzueta, I.; Abanades, J.C.

Decarbonization of Blast Furnace Gases Using a Packed Bed of Ca-Cu Solids in a New TRL7 Pilot. *Energies* **2025**, *18*, 675. <https://doi.org/10.3390/en18030675>

Copyright: © 2025 by the authors. Licensee MDPI, Basel, Switzerland. This article is an open access article distributed under the terms and conditions of the Creative Commons Attribution (CC BY) license (<https://creativecommons.org/licenses/by/4.0/>).

1. Introduction

The steel industry plays a crucial role in the global economy, being indispensable for infrastructure, manufacturing, and transportation. However, it is also one of the most carbon-intensive industries. Steel production is responsible for approximately 7% of global CO₂ emissions, primarily due to the energy-intensive processes required to reduce iron ore into steel. Traditional steelmaking relies heavily on coal, particularly in the blast furnace–basic oxygen furnace (BF-BOF) route, where carbon is used both as a reducing agent and an energy source. Approximately 65% of the world’s steel production is still produced using the BF-BOF route [1]. The chemical reduction of iron ore (Fe₂O₃) using carbon from coke produces a blast furnace gas (BFG) that typically contains around 20–25% CO, 20–25% CO₂, 4–8% H₂ and N₂. For every tonne of pig iron obtained in a blast furnace, approximately 1.8 tonnes of CO₂ are released. The alternative major steel production route uses electric arc furnaces (EAFs), which generate lower CO₂ emissions, but currently make up only about 35% of global steel production [2].

As developing economies continue to grow, global steel demand is projected to increase by 30% by 2050 [3]. Without decarbonization, this growth will lead to higher emissions, counteracting global efforts to reduce GHGs. To stay within the carbon budgets outlined by the IPCC, the steel industry must achieve a near-zero carbon footprint by mid-century [4]. Under these circumstances, it is crucial to rapidly develop and implement efficient CO₂ capture and storage (CCS) technologies at an industrial scale to ensure the sustainability of future steel production.

A wide range of CO₂ capture technologies have been proposed to decarbonize iron and steel production (e.g., chemical absorption, pressure swing adsorption, high-temperature solid looping, membrane separation, etc.), but most of them are still developing well below commercial scale (i.e., TRL \leq 7) [5,6]. To date, the only fully commercial CCS facility for the iron and steel industry is the Al Reyadah plant in Abu Dhabi, with the capacity to produce 3.2 million tonnes of steel per year and operating a capture plant capable of separating up to 1 million tonnes of CO₂ annually. In this factory, CO₂ is captured from a Direct Reduced Iron (DRI) plant using traditional MEA absorption, and this separated CO₂ is subsequently used in Enhanced Oil Recovery (EOR) operations [7].

Unfortunately, there are still no commercial-scale CO₂ capture plants for blast furnace-based steelmaking in operation. Potentially, there is significant difficulty in achieving high CO₂ capture efficiencies in these types of steelmaking plants, as they have multiple sources of carbon emissions, and retrofitting multiple CO₂ capture systems would incur substantial additional costs [8,9]. Blast furnace gas (BFG) alone is responsible for nearly 70% of the emissions from a conventional steel plant. BFG is a residual off-gas with very high carbon content (i.e., CO + CO₂ > 45 vol.%) and a very low heating value (LHV < 3.5 MJ/Nm³), which is primarily used today for on-site power generation and for reheating blast air and coke ovens in order to improve energy efficiency and reduce external energy dependence [10,11]. The possibility of focusing efforts on decarbonizing blast furnace gas (BFG) has emerged as an attractive solution to extend the life of blast furnaces beyond 2050 and meet the decarbonization goals of the steel sector [12].

Pre-combustion technologies are attractive alternatives not only for decarbonizing BFG but also for converting it into a valuable product (i.e., a H₂/N₂ mixture), which can be used as a CO₂-free fuel, as a reducing agent in a DRI process (thus increasing the steel plant's production capacity), or as a feedstock for further chemical transformations (e.g., production of ammonia or synthetic fuels) [13,14]. In this line, sorption enhanced water–gas shift (SEWGS) combines the water–gas shift (WGS) reaction with CO₂ sorption in a single step, converting the CO present in the BFG and steam into a product gas with H₂ and CO₂. In this process, CO₂ is captured by selective adsorption over a hydrotalcite-based material, which shifts the equilibrium of the WGS reaction toward the production of more H₂. The regeneration of the sorbent is achieved by feeding steam, which displaces the adsorbed CO₂, occupying the adsorption sites [15,16]. The feasibility of this pre-combustion technology has been demonstrated up to TR6-7 in dynamically operated packed-bed reactors [17,18].

Among the possible CO₂ sorbents for this type of assisted reforming, gasification and/or WGS reactions for H₂ production, calcium-based solids are attractive due to their wide availability, low cost, fast kinetics and sufficiently high sorption capacity [19,20]. Although the use of CaO for CO₂ capture is well-known [21], it has primarily been developed for post-combustion applications, with most advancements focusing on interconnected fluidized beds [22]. Its development for blue hydrogen production is more limited and mainly focused on using fixed-bed reactors, which allow for pressure swing operation to optimize both H₂ production and CO₂ sorbent regeneration [20,23].

Despite offering theoretical advantages, calcium looping (CaL) has encountered a significant challenge for further development due to the high temperatures required (>850 °C)

for the highly endothermic regeneration of the sorbent. The supply of the large thermal energy needed for CaCO_3 calcination presents a major engineering hurdle, even though this energy can be efficiently recovered during the carbonation and heat recovery stages. One promising alternative is to use O_2 carriers (typically metal oxides) to obtain the heat required for calcination from redox reactions involving these materials (as in chemical looping combustion applications [24,25]). Then, heat is supplied in situ, eliminating the need for air separation units (ASUs) or large heat-transfer surfaces at very high temperatures.

Although various oxygen carriers have been evaluated in combined CaL-CLC applications, including oxides of Ni [26] and Fe [27], copper-based materials present the most favourable features, as the reduction of CuO to Cu is highly exothermic regardless of the fuel type used. Moreover, copper oxide is relatively inexpensive, offering a high theoretical O_2 carrying capacity (about $0.25 \text{ gO}_2/\text{gCuO}$) and excellent reactivity with CO , H_2 and CH_4 [28]. The Ca-Cu looping process for the production of blue hydrogen from natural gas has steadily progressed over the last decade, reaching process validation at TR4-5 [29].

The calcium-assisted steel-mill off-gas hydrogen (CASOH) process is an adaptation of the Ca-Cu looping aimed at decarbonizing steel mill off-gases while separately producing a hydrogen-enriched gas and nearly pure CO_2 [30]. A simplified scheme of the CASOH process is illustrated in Figure 1. The main stage of the process is the CASOH itself, where the CO contained in the BFG (between 20 and 25 %vol.) reacts with steam to produce H_2/N_2 gas. The Cu-based material catalyses the WGS reaction, while the majority of the CO_2 , both generated during the stage and initially present in the BFG, reacts with CaO to form CaCO_3 . The removal of CO_2 from the reacting atmosphere shifts the equilibrium toward increased H_2 production. A very high conversion of the inlet CO is feasible at temperatures between 550 and 700°C , giving as a result a product gas with 35–40 %vol. H_2 diluted in N_2 and very low amounts of CO and CO_2 .

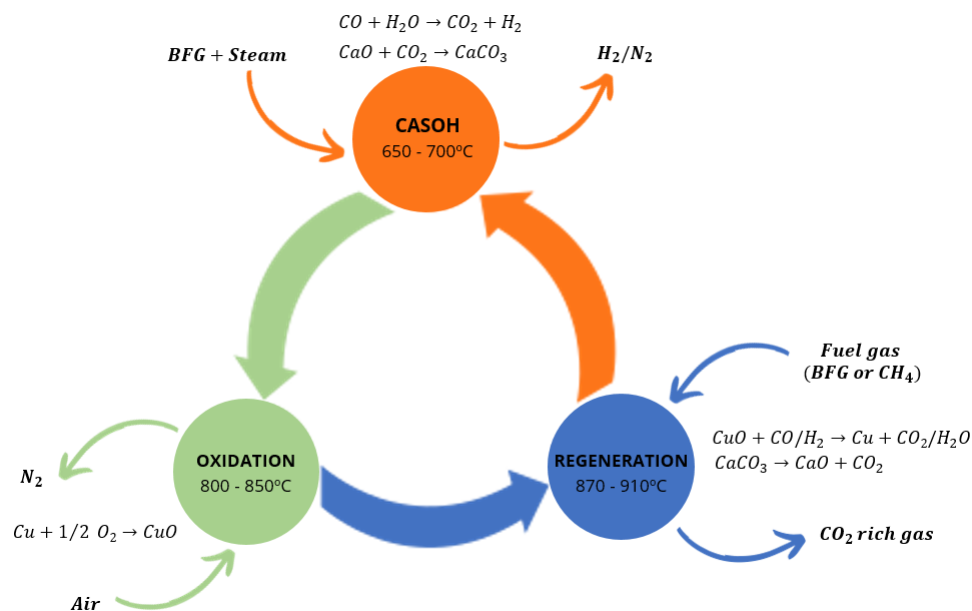


Figure 1. Scheme of the CASOH process for the decarbonization of BFG and the production of H_2 -rich gas.

To regenerate the carbonated CO_2 sorbent, two additional redox stages are needed, where a Cu/CuO looping supplies the heat required to reach the appropriate temperatures to carry out the calcination of CaCO_3 . Therefore, there is a second stage in the process that involves the oxidation of Cu-based material to CuO using air. This exothermic reaction

increases moderately the bed temperature to prevent premature calcination of CaCO_3 and avoid some CO_2 leakage, which would reduce the CO_2 capture efficiency of the process.

In the final stage, CuO is reduced to Cu , preferably by reacting with BFG, although other steelmaking gases containing CO , H_2 , and/or CH_4 , or natural gas can also be used. The heat generated during CuO reduction raises the temperature to nearly $900\text{ }^\circ\text{C}$, enabling the decomposition of CaCO_3 into CaO and CO_2 . Under these conditions, the fuel gas is fully converted to CO_2 and steam, yielding a CO_2 -rich gas. Once this stage is complete, the reactor contains reduced Cu able to catalyse the WGS reaction and active CaO to capture CO_2 in a new CASOH cycle. Enhanced versions of the CASOH process are under investigation by implementing vacuum pressures to the calcination stage.

The feasibility of the CASOH process has already been experimentally demonstrated at $\text{TRL} \leq 4$ [31,32]. A key objective of the C4U project [33] is to carry out the proof of the concept at $\text{TRL}7$ when treating real blast furnace gas from an Arcelor Mittal factory located in Asturias (Spain). The same functional CaO - and Cu -based materials previously used at a smaller scale have been employed in the experimental campaigns at the $\text{TRL}7$ pilot plant. This work outlines the commissioning activities and the first experimental results obtained in the pilot plant. Once the design of the pilot was finalized at the end of 2021, construction began at the GasLab industrial R&D testing site of Arcelor Mittal Asturias. Following the commissioning works, the pilot successfully generated its first $\text{TRL}7$ results in the first half of 2024, which are relevant for all gas–solid reactions involved in the CASOH process, accumulating over 550 h of operation.

2. Description of the CASOH Pilot Plant and Summary of the Commissioning Activities

The CASOH pilot plant has been designed to allow high temperature operation (up to $1000\text{ }^\circ\text{C}$) within the bed of solids. The key component is the packed-bed reactor, measuring 5 m in height and 0.5 m in inner diameter, which complies with the $\text{TRL}7$ standards for pre-combustion systems. That is, the plant can handle a flow of BFG equivalent to approximately 1 MWth, divided into $300\text{ Nm}^3/\text{h}$ of upgraded BFG and about 0.7 MWth of sensitive heat produced at high temperature. The reactor, with a capacity to hold up to 1 ton of solids, has been engineered to accommodate temperature swings expected in future multi-reactor systems, following the principles of commercial high-temperature solid looping-based capture systems, while adapting to the high-temperature conditions characteristic of the CASOH process.

Figure 2 shows the Process Flow Diagram (PFD) for the CASOH pilot. This PFD illustrates the pilot equipment along with the supply lines for blast furnace gas (BFG), natural gas (NG) (used both for the CASOH process and the flare), steam, and nitrogen (N_2), all sourced directly from the ArcelorMittal GasLab utilities network. Additionally, the air and carbon dioxide (CO_2) required for the process are provided by a compressor (COMP) and pressurized cylinders, respectively. The PFD also includes the cooling water circuit for the reactor's product gases, as well as the gas sampling system linked to two gas analysers, enabling the measurement of gas composition at various points within the pilot plant. BFG is fed into the pilot via BLOWER 1 at up to 4 bara, near ambient temperature, and saturated with water. It enters through the on/off valve V13, with flow regulated by the mass flow meter MF1 and control valve FCV1. The non-return valve NRV1 prevents reverse flow, while pressure-regulating valve PRV2 limits pressure to 1.5 bara (i.e., the maximum pressure allowed according to gas preheater specifications). During specific operations, BFG can bypass the reactor and flow directly to the flare by adjusting valves V17 and V12. Thermocouple T3 monitors the BFG (or NG) temperature before entering the reactor. To meet ATEX safety requirements, the preheaters (PREH in Figure 2) are

positioned over 1.5 m from the BFG entry. This distance has been gained by means of a two-meter refractory-lined pipe that connects the preheaters to the reactor inlet, omitted from the PFD for simplicity.

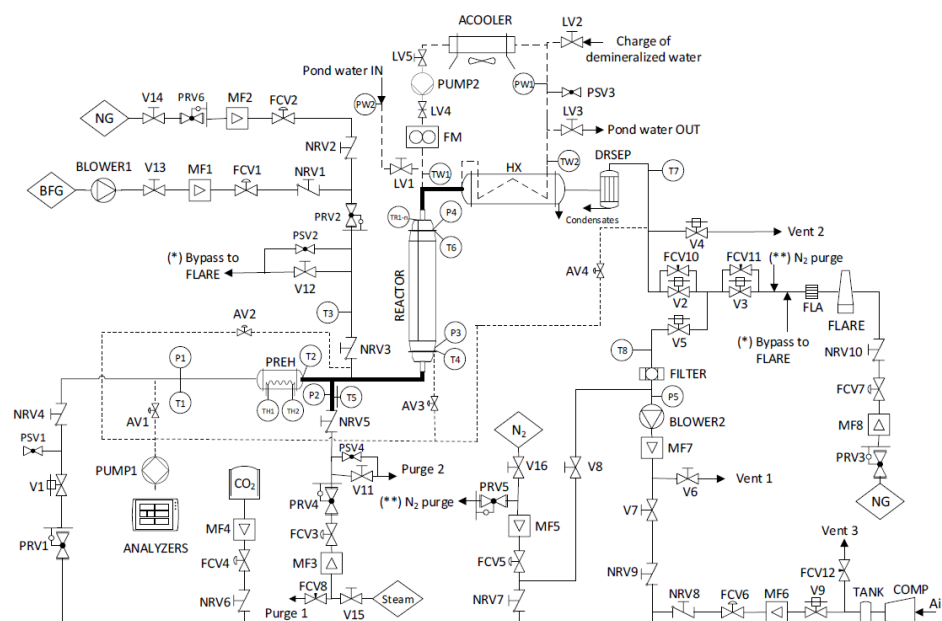


Figure 2. Process flow diagram (PFD) of the CASOH pilot. Secondary lines for bypassing BFG and N_2 to the flare are partially omitted in the PFD for simplicity. (*) and (**) mark the missing section's start and end points.

On the other hand, steam from the AMA utility, at $150\text{ }^{\circ}\text{C}$ and 2 bara, enters the pilot via valve V15. The flow control valve FCV8 is used to purge initially the line. To obtain a stable flow of steam during operation, the valve V11 is initially open, whereas the flow of steam is regulated by means of the orifice plate flow meter MF3 and the associated control valve FCV3. Once condensate-free flow is ensured, FCV8 and V11 are closed, and valve V18 must be open to feed steam, which is connected near the BFG inlet. The non-return valve NRV5 prevents reverse flow, with thermocouple T5 and pressure sensor P2 monitoring steam temperature and pressure. The air necessary for the pilot operation, primarily during copper oxidation and bed preheating, is supplied by a compressor (COMP). A 3000 L buffer tank (TANK) ensures stable flow of air. Air enters the pilot through on/off valves V9 and V1, with flow regulated by mass flow meter MF6 and control valve FCV6. Non-return valves NRV8 and NRV4 prevent reverse flow, while pressure-regulating valve PRV1 limits the pressure to 1.5 bara, and safety valve PSV1 purges gas if overpressure occurs. Thermocouple T1 and pressure sensor P1 monitor the gas temperature and pressure before it enters the preheaters (PREHs). The gas preheaters are arranged in parallel and have a combined power of 80 kW ($2 \times 40\text{ kW}$). Although they can reach an outlet temperature of $1100\text{ }^{\circ}\text{C}$, the gas temperature is limited to $700\text{ }^{\circ}\text{C}$ due to the restrictive design temperature of the refractory-line pipe used to connect PREHs with the reactor. Thermocouples TH1 and TH2 monitor the temperature in each preheater, while thermocouple TH3 measures the exit gas temperature.

With respect to N_2 supply, it enters through the on/off valve V16, which splits the line into two paths. One directs N_2 to the flare for purging, with pressure regulated to 1.2 bara by valve PRV5. The other supplies N_2 for plant operations through the reactor, with flow controlled by the mass flow meter MF5 and valve FCV5. The non-return valve NRV7 prevents reverse flow in the line. As mentioned above, the CO_2 required for the process is supplied from pressurized cylinders. The flow of CO_2 is regulated using the insertion

probe mass flow meter MF4 and the corresponding control valve FCV4. Additionally, the non-return valve NRV6 prevents any reverse flow in this line. Moreover, the pilot plant has two natural gas inlets: one supplies NG for operations through the reactor, and the other feeds the flare. Pressure in each line is regulated by valves PRV6 and PRV3. The NG for the process enters via on/off valve V14, with flow managed by the mass flow meter MF2 and control valve FCV2. The non-return valve NRV7 prevents reverse flow in the line.

In every stage of the CASOH process, the gas streams enter the packed-bed reactor from the bottom, with product gas exiting from the top. The axial temperature within the reactor is monitored using three multipoint thermocouples, measuring at 22 points (TR1-10, TR2-10, T4, and T6). Pressure at the reactor's top is gauged by sensor P4, while P-Diff measures pressure drop across the bed. The product gas after the reactor circulates through the heat exchanger (HX), where it is cooled down to around 25–30 °C. The cooling fluid is demineralized water that circulates in a closed loop (flow rate around 165 L/min) at a pressure of around 1.5 bara (measured in PW1), and it is refrigerated by means of the air cooler ACOOLER composed of six fans. The thermocouples TW1 and TW2 measure the temperature of the cooling water at the inlet and the outlet of the heat exchanger, respectively. In case of failure in the circulation of the demineralized water, the on/off valve LV1 is opened to feed pond water to the cooling circuit, which flows in an open circuit and is finally discharged through the on/off valve LV3. After cooling, the product gas passes through a drop separator (DRSEP) to remove liquid water before either being vented via V4 (if the gas contains air, N₂ and/or CO₂) or sent to the flare for combustion via V3 and V5 (if the gas contains CO, H₂, CH₄). Finally, flow control valves FCV10 and FCV11 manage overpressure in case of malfunction of V2 or V3.

The commissioning of the CASOH pilot plant faced significant delays due to challenges typical of TRL6-7 scale projects, exacerbated by the COVID-19 pandemic and supply chain issues. Most of the initial testing hours were focused on adjusting pilot equipment and instruments, recalibrating systems, addressing gas leaks under increasingly demanding conditions, repairing damage from the first high-temperature trials, including a broken gas preheater and malfunctioning gaskets, and resolving communication and logic issues between components (such as the torch and compressor) and the control system, all essential for ensuring safe operation of the pilot. Despite these hurdles, the plant achieved its first successful decarbonization of BFG in May 2024. The observed gas concentration trends and temperature profiles in the packed bed during these full cycle tests (see Section 3) have been qualitatively consistent with previous tests carried out in lower TRL rigs with the same Ca-Cu functional materials.

As part of the commissioning of the pilot plant, and prior to conducting reaction experiments under CASOH process conditions, moderate temperature tests were performed to gain confidence in the pilot's operability and to calibrate the thermal insulation in the reactor. These preliminary tests were designed to activate the bed of solids by calcining a portion of the CaCO₃ to CaO. For safety reasons, the initial reduction of CuO with BFG was conducted at relatively mild starting temperatures of around 400 °C. The subsequent calcination of CaCO₃ was carried out using only the thermal power available from the pilot's electric preheater, supplying air or N₂ at 700 °C to the bed of solids. An inspection conducted with an infrared camera when maximum temperatures were reached in the reactor revealed that the wall temperatures remained well below 100 °C, confirming the high quality of the thermal insulation in the chemically active bed of solids (see Figure 3).

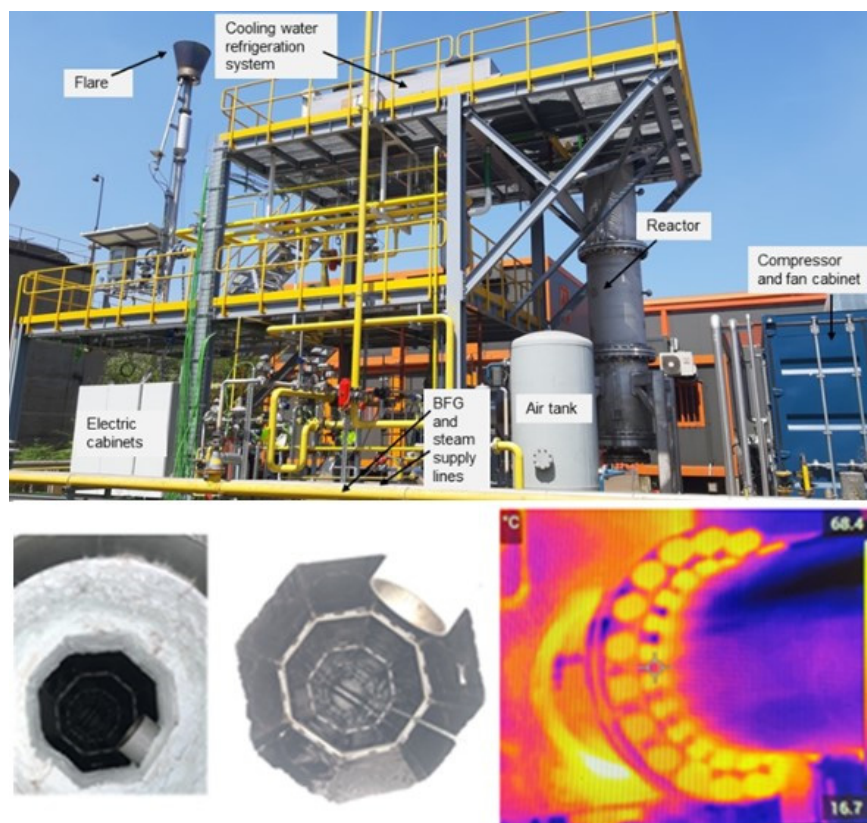


Figure 3. Final overview of the CASOH pilot fully commissioned, with the interior of the reactor observed from the top and external temperature mapping during operation at high temperatures.

3. Results and Discussion

For the first experimental campaign, the fixed-bed reactor was loaded with approximately 50 kg of alumina (Al_2O_3), which serves as both the support and gas distributor for the reactive bed. Above this, there was a limited quantity of Ca/Cu materials in the bed of solids (about 200 kg of mixed solids using CaCO_3 provided by Carmeuse and Cu-supported catalyst supplied by Johnson Matthey, London, UK). These solids formed a reacting bed height of about 1 m, while future tests are expected to aim for more stable operations with taller beds of up to 5 m.

The CASOH pilot has accumulated over 550 h of valuable operational experience to date. Tests have been conducted under various initial bed temperature profiles, gas residence times, and gas compositions during both the CASOH stage (with and without steam) and the calcination–reduction stages, including O_2 levels during the Cu oxidation stage. The results presented in this work showcase successful reaction stages of the process, including CASOH, Cu oxidation, CuO reduction, and CaCO_3 regeneration. A summary of the experimental conditions of the main stages is presented in Table 1 to provide a clearer overview of the experimental conditions used during these tests.

The gas inflow rates were selected to ensure that, for the given reactive bed length, the gas residence times would align with those anticipated in industrial-scale CASOH reactors (approximately 1.5–2 s). As for the initial bed temperatures, a value of 600 °C was chosen for the CASOH stage, as it allows for both high CO_2 capture efficiency and the maximum achievable H_2 concentration, consistent with the WGS equilibrium when CaO is present to assist the reaction. For the subsequent stages involving Cu oxidation and regeneration, the initial temperature profiles were chosen to reflect the conditions expected during cyclic operation of the CASOH process, ranging between 600 and 800 °C.

Table 1. Summary of experimental conditions for CASOH, Cu oxidation and regeneration stages.

Conditions	Value
Solids bed properties	
Quantity of Ca/Cu materials in the bed of solids, kg	200
Length of solids bed in the reactor, m	1
Reactor diameter, m	0.5
CASOH stage	
Initial bed temperature, °C	600
Pressure, bar	1
S/CO molar ratio	2
Feed temperature, °C	600
Inlet total flow rate, Nm ³ /h	91
Inlet Steam, N ₂ , BFG flow rate, Nm ³ /h	15, 38, 38
Inlet BFG composition CO, CO ₂ , H ₂ , N ₂ , %vol.	21, 22, 7, 50
Maximum gas velocity, m/s	0.5
Residence time of the gas, s	2
Cu oxidation stage	
Initial bed temperature, °C	735–760
Pressure, bar	1
Feed temperature, °C	640
Inlet total flow rate, Nm ³ /h	106
Inlet Air, N ₂ flow rate, Nm ³ /h	52, 54
Inlet composition O ₂ , N ₂ , %vol.	12, 88
Maximum gas velocity, m/s	0.6
Residence time of the gas, s	1.7
Regeneration (CuO Reduction/CaCO ₃ calcination) stage	
Initial bed temperature, °C	600
Pressure, bar	1
Feed temperature, °C	600
Inlet total flow rate, Nm ³ /h	98
Inlet N ₂ , BFG flow rate, Nm ³ /h	52, 46
Inlet BFG composition CO, CO ₂ , H ₂ , N ₂ , %vol.	20, 23, 6, 51
Maximum gas velocity, m/s	0.55
Residence time of the gas, s	1.8

Before proceeding with the CASOH stage detailed below, a partial calcination of CaCO₃ was performed by introducing a sufficient flow rate of N₂ at an inlet temperature of 750 °C. The degree of calcination was monitored by measuring CO₂ concentration in the outlet gas. Once approximately 70 moles of active CaO for CO₂ capture were generated, the calcination stage was concluded. Subsequently, N₂ was fed at around 600 °C for 2 h to stabilize the bed temperature for optimal CASOH operation. In the described CASOH stage, a BFG flow rate of 38 Nm³/h was introduced, consisting of roughly 21% CO, 22% CO₂, 7% H₂, and 50% N₂ (%vol.). A steam flow of 15 Nm³/h was also added to maintain a S/CO ratio close to 2 in the feed. Additionally, a nitrogen flow of 38 Nm³/h was directed through the preheaters to ensure safe operation, maintaining a minimum gas flow while the heaters operated at high temperatures and prevented the flow of combustible gas and steam toward them. During the experiment, the temperature of the N₂ across the preheaters (TH1 and TH2) stabilized at 725 °C, giving as a result a temperature of N₂ after the preheaters (TH3) at 590 °C. Under these conditions, the total inlet gas flow reached 91 Nm³/h, resulting in an approximate gas velocity inside the reactor of 0.5 m/s and a residence time of about 2 s.

Figure 4 shows the evolution of the product gas composition during the CASOH stage. This composition excludes the additional N₂ added to the feed to ensure the safe operation of the gas preheaters. During the first 5 min (the pre-breakthrough period), the BFG was nearly fully decarbonized, yielding a hydrogen-enriched stream. The kinetics of the water–gas shift (WGS) and CaO carbonation reactions were highly favourable under

these experimental conditions, achieving nearly complete CO conversion and a very high CO₂ capture rate. CO and CO₂ concentrations in the product gas dropped below 2% vol (on a dry basis), indicating a CO₂ capture efficiency above 95%. The removal of CO₂ from the gas phase enhanced H₂ production, reaching a maximum concentration of 40% vol. (on a dry basis) in the product gas, which aligns with the WGS equilibrium, aided by the simultaneous carbonation of CaO.

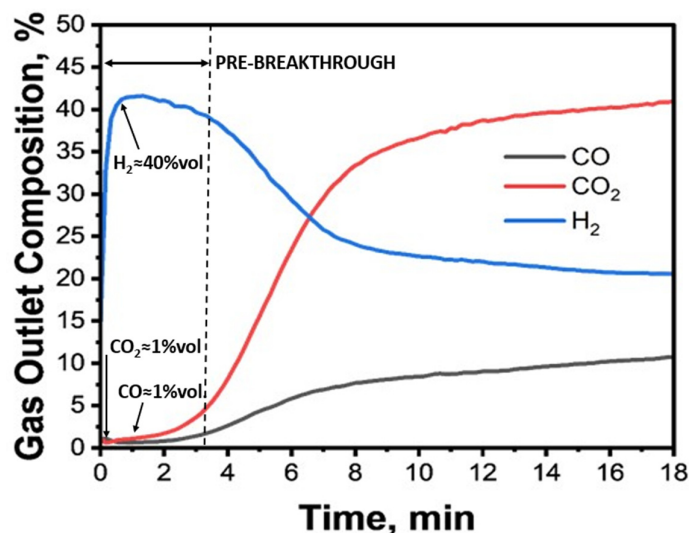


Figure 4. Evolution of the composition of the product gas during the CASOH stage.

After 5 min, the carbonation front approached the end of the reacting bed, resulting in a gradual decrease in H₂ concentration alongside an increase in CO and CO₂ concentrations. By just over 10 min into the operation, the CO₂ sorbent was nearly fully carbonated and ceased capturing CO₂. From that point, the fixed bed functioned as a conventional WGS reactor, producing a gas with approximately 22% vol. H₂, 10% vol. CO, and 40% vol. CO₂ in nitrogen.

As illustrated in this example of the CASOH stage, during the period before the breakthrough curve appears in the product gas concentration, very high CO₂ capture efficiencies are achieved, comparable to those attained in other CO₂ capture processes (see Table 2). The key advantage of the CASOH process compared to most capture technologies applied to steel mills (a feature shared with SEWGS) is that it not only decarbonizes a low-energy-value gas (BFG), but also produces a hydrogen-enriched gas. This product can be used as a reducing agent in the steelmaking process, reducing the demand for coke in the blast furnace, serving as a CO/CO₂-free fuel, or acting as a feedstock for chemical synthesis. Table 2 also compares the technology readiness level (TRL) of major capture technologies applied to steel mills with the CASOH process.

Table 2. Comparative CO₂ capture Efficiency and current TRL of the proposed CASOH process versus other CO₂ capture technologies for decarbonizing in iron and steel plants.

Technology	CO ₂ Capture Efficiency (%)	TRL [11]
CASOH	>95	7
Chemical absorption	>95 [16]	9
Adsorption, PSA	90–99 [34,35]	7
Oxy-blast furnaces	>90 [11]	7
SEWGS	>95 [17]	7
Membrane	90–98 [36]	5

On the other hand, Figure 5 depicts the temperature evolution at different points in the reactor during the CASOH stage. The thermocouple TR_i indicates the heating of the reactive bed in the second half of the fixed-bed reactor. When half of the CASOH stage had elapsed, the thermocouple at a height of 0.5 m began to show a rapid temperature increase due to the heat generated by the exothermic WGS and CaO carbonation reactions. As the CASOH stage progressed, the temperature at this point rose to a maximum of approximately 780 °C. Since the carbonation front advanced more quickly than the heat exchange front, the carbonated material was left behind at the maximum temperature, keeping the temperature at TR_{0.5m} close to 780 °C throughout the entire CASOH stage. Meanwhile, thermocouples positioned higher in the solids bed (i.e., TR_{0.6m} and TR_{0.65m}) gradually increased in temperature as they were reached by the carbonation front, exhibiting a temperature trend similar to that observed at TR_{0.5m}.

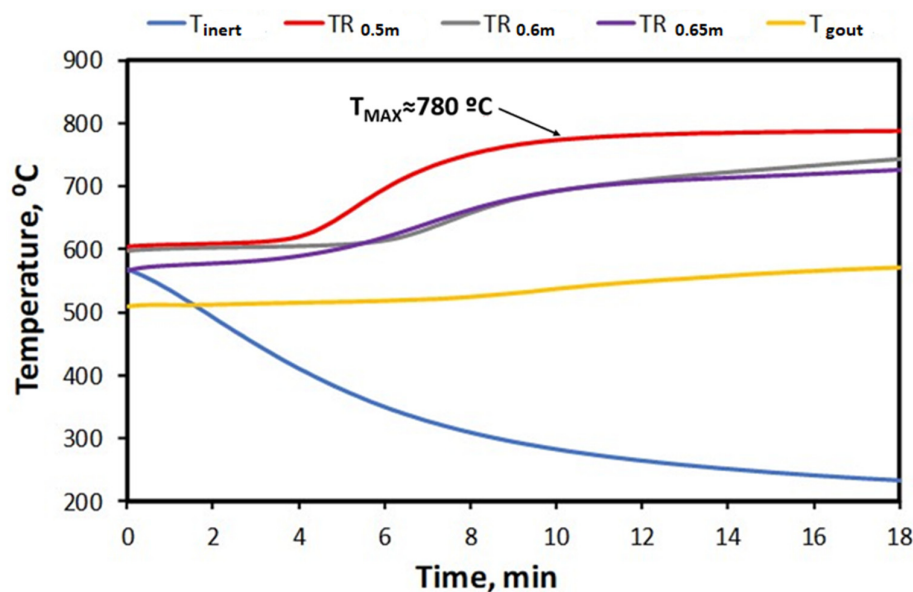


Figure 5. Evolution of the temperature profiles at different points of the packed-bed reactor during the CASOH stage.

As the carbonation front advanced rapidly, leaving behind the heat released by the reaction, the product gas was only slightly heated during the CO₂ capture period (i.e., during the first 8 min of operation), exiting at temperatures close to the initial values in the bed. T_{gout} in Figure 5 is positioned at the top of the reactor, where no solids are present, and remained stable at around 515 °C during this period. Only when the carbonation front reached the end of the bed did the temperature at T_{gout} begin to rise significantly, eventually exceeding 570 °C by the end of the stage. The temperature evolution (T_{inert}) in the portion of the bed containing alumina (at the reactor inlet) exhibited a different trend during the CASOH stage. Initially, this section of the inert bed was at around 570 °C due to prior temperature conditioning with preheated N₂. However, once the reaction stage commenced and predominantly cold gases were introduced into the reactor (since neither BFG nor steam could be preheated in PREH), the temperature in the inert bed gradually decreased, dropping below 300 °C by the end of the CASOH stage.

The results obtained in a Cu oxidation stage using air are described below. This stage was preceded by a CASOH phase and a brief 5 min nitrogen purge to clear any residual fuel gas from the pilot plant lines. Consequently, at the start of this stage, the copper material was in its metallic form (Cu), and the calcium material was fully carbonated. In this oxidation stage, a flow of 52 Nm³/h of air was introduced, along with an additional 54 Nm³/h of nitrogen, resulting in a total inlet gas stream of 106 Nm³/h with an oxygen

concentration of 12% vol. Under these conditions, the maximum gas velocity within the reactor reached 0.6 m/s, leading to a residence time of approximately 1.67 s, which aligns with the expected conditions for a CASOH process reactor at an industrial scale. During the operation, the temperature of inlet gas remained stable around 640 °C.

Figure 6 presents the composition of the reactor's exit gas during this stage. During the initial 10 min of operation, the oxygen in the inlet gas was almost completely consumed, with O₂ concentrations falling below 0.5% vol. This indicates the extremely rapid kinetics of copper oxidation, even with such short gas residence times. After this period, as the oxidation front reached the end of the bed, the O₂ concentration in the exit gas began to rise quickly, matching the inlet value (12% vol.) within just 3 min, marking the breakthrough period. This sharp oxidation profile highlights the excellent reactivity of the copper material with oxygen.

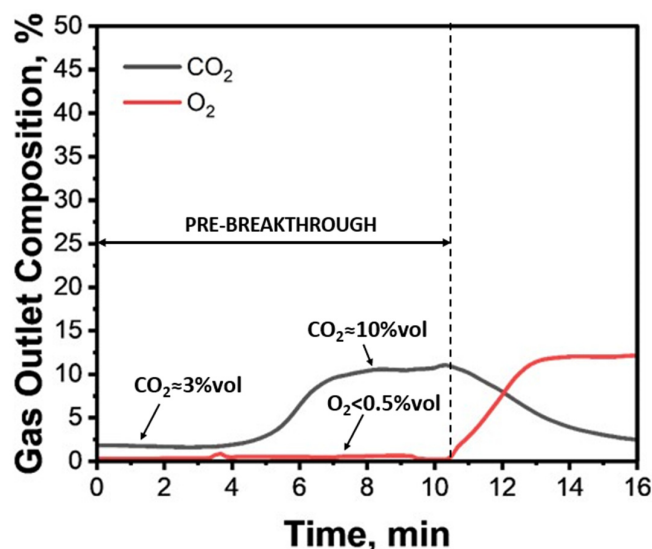


Figure 6. Evolution of the composition of the product gas during the oxidation stage.

Additionally, the heat generated during the oxidation reaction caused a temperature increase, leading to partial calcination of the CaCO₃ present in the bed. As shown in Figure 6, CO₂ concentrations in the product gas were below 3% at the beginning of the stage, indicating that the bed had not yet reached temperatures high enough for significant calcination. However, after 5–6 min of operation, CO₂ levels rose substantially, peaking at around 10% vol. in the product gas. Based on these CO₂ concentrations, it is estimated that nearly 60 moles of the CaCO₃ initially present in the reactor were calcined. This represents a notable loss of CO₂, which could be mitigated by operating at higher pressures, as designed for the CASOH process on an industrial scale. Furthermore, proper heat management of the bed, including effective cooling and heating stages with gas recycling before oxidation, could minimize CO₂ release to below 1% vol. during copper oxidation. Once a stable O₂ concentration of 12% vol. (equal to the inlet gas) was observed in the product gas, it indicated that all the copper in the bed had been oxidized, signaling the completion of the stage.

Figure 7 illustrates the temperature profiles at various points within the reactor during the oxidation stage. The thermocouples embedded in the reactive bed (TRi) showed that the reactive solids started at temperatures between 735 °C and 760 °C, due to the preceding CASOH and N₂ purge stages. As oxidation proceeded, the front moved in a narrow band. The TR_0.5m thermocouple did not detect significant temperature changes until about halfway through the stage, when a sharp temperature increase was recorded. Within approximately one minute, the temperature peaked at 871 °C, reflecting a rise of around

110 °C due to the heat released during copper oxidation. As the oxidation front advanced, similar heating was observed in downstream thermocouples.

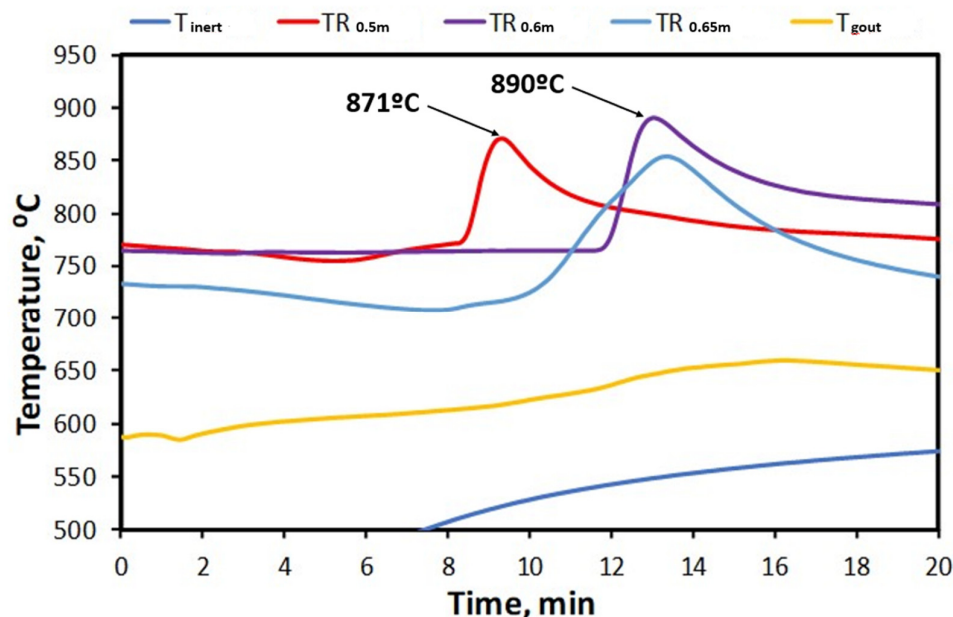


Figure 7. Evolution of the temperature profiles at different points of the packed-bed reactor during the oxidation stage.

Despite the rapid oxidation front movement and substantial heat generated, the gas temperature at the outlet (T_{gout}) showed only a slight increase throughout the process. It was not until the oxidation front approached the end of the bed that T_{gout} began to rise slightly, eventually exceeding 658 °C by the end of the stage. The temperature of the alumina bed at the reactor's bottom (T_{inert}) gradually increased during this stage, starting at nearly 300 °C due to the introduction of low-temperature blast furnace gas (BFG) and steam during the preceding CASOH stage. The preheated air/ N_2 feed subsequently raised the temperature of the inert material, which reached nearly 575 °C by the end of the oxidation phase.

To conclude this section, an example of a CuO reduction stage using BFG with simultaneous calcination of $CaCO_3$ is described. This CuO reduction stage was preceded by a preheating period using air and nitrogen, followed by a final nitrogen purge to eliminate any residual oxygen from the pilot plant lines. During the preheating phase, the temperatures in the preheaters (TH1 and TH2) were maintained at 700 °C, resulting in a gas outlet temperature from the preheaters of approximately 600 °C. This ensured that the reactor was heated to around 600 °C, which is a suitable temperature for initiating the reduction of CuO with BFG. To carry out the reduction of the CuO-based material present in the reactor, a flow of 46 Nm^3/h of BFG was introduced, mixed with 52 Nm^3/h of preheated nitrogen (i.e., a total gaseous feed of 98 Nm^3/h). The BFG supplied by the steel mill in that moment contained 20% CO, 23% CO_2 , 6% H_2 , and 51% N_2 (%vol.). Under these operating conditions, the gas achieved a maximum velocity of nearly 0.55 m/s in the reactor, resulting in a residence time of approximately 1.8 s.

Figure 8 illustrates the gas composition at the reactor outlet during the whole reduction stage (excluding the extra N_2 added in the feed to ensure the safe operation of the gas preheaters). As can be seen, there was a notable increase in CO_2 concentration in the product gas, peaking at around 65% vol. on a dry basis. During the pre-breakthrough period, almost all of the CO and H_2 in the incoming BFG was converted, with outlet levels of these gases falling below 0.2% vol. on a dry basis. The CO_2 concentration in the

product gas, combined with the measured gas flow rate to the torch, indicated that partial calcination of CaCO_3 occurred alongside the reduction of CuO by the CO and H_2 in the BFG. The expected concentration of CO_2 in the product gas solely due to the oxidation of BFG would be 43% vol. (on a dry basis and excluding additional dilution with N_2), rather than the values close to 65% CO_2 measured during this period.

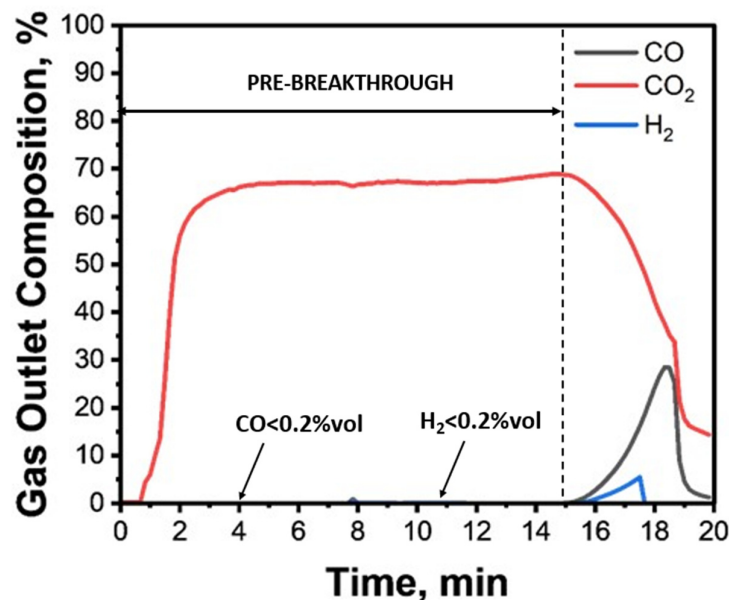


Figure 8. Evolution of the composition of the product gas during the CuO reduction stage.

Additionally, based on the inlet flow rates and excluding the H_2 oxidized to H_2O (retained in the drop separator), the expected outlet flow to the torch was around $95 \text{ Nm}^3/\text{h}$. However, an actual flow of approximately $105 \text{ Nm}^3/\text{h}$ was observed during the experiment. This excess of $10 \text{ Nm}^3/\text{h}$ confirmed that, in addition to the CuO reduction, there was simultaneous partial calcination of CaCO_3 , a process consistent with the classical regeneration stage of the CASOH process. After extending the operation for an additional 5 min, a significant rise in CO and H_2 concentrations, coupled with a drop in CO_2 , was observed in the outlet gas. This shift indicated that the CuO reduction front was nearing the end of the reactive solid beds. Following a rapid breakthrough period lasting about 2–3 min, the CuO reduction stage concluded after 19 min of operation. By this point, the product gas composition closely resembled that of the inlet gas. Based on the excess CO_2 and the observed flow rates during the pre-breakthrough period, it was estimated that around 120 moles of CaCO_3 were calcined during the CuO reduction stage.

On the other hand, Figure 9 illustrates the temperature evolution at various points in the reactor during the CuO reduction stage. The initial temperature profile of the bed was around $600 \text{ }^\circ\text{C}$. As observed in previous stages, during the first half of the stage, the temperature measured by thermocouples located in the latter half of the bed remained constant. This indicates that the reduction front advanced ahead of the heat exchange front, so all the heat generated from the reduction of CuO to Cu remained in the solids behind the reaction front. After 9 min of operation (approximately half of the total duration of the stage), the thermocouple positioned at the middle of the bed ($\text{TR}_{0.5 \text{ m}}$) experienced a sudden temperature increase as it was reached by the reduction front. This sharp temperature rise confirms the rapid kinetics of CuO reduction with CO and H_2 present in the BFG. Thermocouples located further along the bed showed a similar trend, reaching a maximum temperature of up to $820 \text{ }^\circ\text{C}$ at $\text{TR}_{0.65 \text{ m}}$. As seen in other stages, once the reaction front moved through a section of the reactor, the converted solids stabilized at

this maximum temperature, creating a heat plateau. In contrast, the lower section of the reactor, occupied by inert alumina, exhibited a different temperature behaviour. As with the CASOH stage, the temperature (T_{inert}) gradually decreased when the BFG + N_2 gas mixture was introduced, since the BFG was fed directly without preheating.

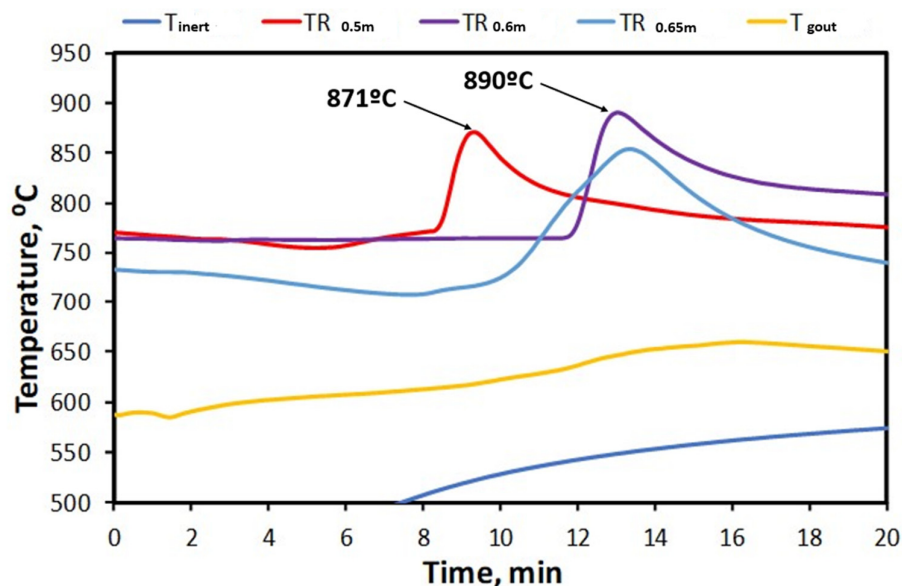


Figure 9. Evolution of the temperature along the packed-bed reactor during the CuO reduction stage with BFG.

Table 3 summarizes the characteristics of the product gases obtained during stable periods in every stage of the CASOH process for the conditions shown in this work.

Table 3. Characteristics of the product gases obtained in the CASOH process during pre-breakthrough periods.

Conditions	Value
CASOH stage	
Maximum bed temperature, °C	780
Outlet gas comp. (dry basis): H_2 , CO, CO_2 , N_2 , %vol.	40, 1, 1, 58
CO conversion, %	>95%
CO_2 capture efficiency, %	95
Cu oxidation stage	
Maximum bed temperature, °C	871
Outlet gas composition: O_2 , N_2 , %vol.	0.5, 95
O_2 conversion, %	>97%
Regeneration (CuO reduction/ $CaCO_3$ calcination) stage	
Maximum bed temperature, °C	820
Outlet gas comp. (dry basis): CO_2 , CO, H_2 , N_2 , %vol.	65, 0.2, 0.2, 34.6
CO conversion, %	>98%
H_2 conversion, %	>96%

These experimental results provide the first demonstration of the viability of each stage of the CASOH process using actual steelworks gases as feed for the fixed bed reactor at TRL7. A successful initial experimental campaign has been completed, accumulating over 550 h of operation while utilizing only 1 m of the total possible 5 m of bed height. These findings have confirmed, at a larger scale, observations previously made with functional materials at lower TRLs. Additionally, a first validation of the CASOH reactor models will be conducted using experimental data obtained at TRL7, providing confidence for the reactor and process scale-up, which will be further validated during the remaining tests

planned until the end of the project. The upcoming experimental campaigns will involve a solid loading of over 600 kg, resulting in a bed height of 3.5 m. The goal is to confirm the viability of the CASOH process with higher flow rates and longer operating periods, aiming to accumulate up to 2000 h of operation by the end of the C4U project.

4. Conclusions

The first complete, safe and successful operation of the TRL7 CASOH pilot has been carried out for the first time using actual steel mill off-gases, accumulating over 550 h of operation experience. The feasibility of every stage of the CASOH process (i.e, CASOH, Cu oxidation and sorbent regeneration) has been demonstrated using the first batch of 200 kg of commercial Ca- and CuO-based materials. During the CASOH stage, the blast furnace gas was almost entirely decarbonized and converted into a product gas containing up to 40% vol. H₂ diluted in N₂. The removal of CO₂ shifted the water–gas shift (WGS) equilibrium, maximizing hydrogen production and achieving nearly complete conversion of CO, resulting in CO₂ capture efficiency exceeding 95% during this stage. The Cu-based material demonstrated excellent reactivity in both the oxidation and reduction stages, leading to short breakthrough periods and rapid increase in temperatures at the reaction fronts. During the oxidation stage, almost 100% conversion of O₂ was achieved, and in the regeneration stage, both CO and H₂ were fully converted during the pre-breakthrough period, yielding a product gas enriched with CO₂ (up to 65% by volume) with no unconverted combustible gases present. The outstanding results achieved at the laboratory scale [31,32], including H₂ yield and CO₂ capture efficiency during the CASOH stage, as well as BFG conversion and CO₂ purity during the regeneration stage, have also been successfully replicated in the TRL7 pilot. Moreover, the breakthrough curves and temperature profiles observed in each stage closely match those obtained at smaller scales. Moreover, the TRL7 pilot successfully operated under dynamic conditions with varying gas residence times and compositions. The experimental data indicate that the reactor can handle fluctuations in temperature and gas composition, demonstrating its robustness and adaptability. The promising preliminary findings obtained from a one-meter-high bed indicate that increasing the bed height and solid loading would make the CASOH process scalable. In the latest experimental campaigns, the bed has been loaded with more than 600 kg of a mixture of calcium and copper solids, reaching a height of 3.5 m, which significantly improves the operational performance of the process. The planned experiments, whose results will be detailed in future publications, aim to improve operational throughput and assess the process's long-term viability, paving the way for eventual scale up. Scaling this process to an industrial level will primarily involve addressing several challenges: First, ensuring that calcium and copper materials maintain sufficient activity after thousands of hours of operation and exposure to repeated cycles in the presence of impurities from blast furnace gas. Additionally, it will be critical to demonstrate the efficient implementation of the process in multi-bed reactors, where each reactor operates in parallel, sequentially completing each stage of the process and continuously producing H₂-enriched gas (CASOH stage), a N₂-rich stream (Cu oxidation stage), and a CO₂-rich gas (regeneration stage). Finally, seamless integration of the process within the steel plant will be crucial to utilizing residual heat from both the steel mill and the CASOH process for preheating the inlet gases, thereby optimizing the energy efficiency of the CASOH process.

Author Contributions: Conceptualization, J.R.F., M.C. and J.C.A.; methodology, J.R.F. and M.A.; validation, A.M., M.D., R.G. and I.A.; formal analysis, M.A. and M.D.; investigation, A.M. and R.G.; data curation, M.A., R.G. and M.D.; writing—original draft preparation, J.R.F. and M.D.; writing—review and editing, J.C.A.; visualization, J.R.F., M.A.; supervision, M.C., I.A. and J.C.A.;

project administration, M.C. and J.C.A.; software, A.M.; resources, I.A.; funding acquisition, M.C. and J.C.A. All authors have read and agreed to the published version of the manuscript.

Funding: The authors acknowledge the financial support from the C4U Project funded by the European H2020 Programme under Grant Agreement no 884418. We acknowledge additional funding from CSIC's Interdisciplinary Thematic Platform (PTI+) Transición Energética Sostenible+ (PTI-TRANSENER+) as part of the CSIC program under the Spanish Recovery, Transformation and Resilience Plan funded by the Recovery and Resilience Facility of the European Union, established by the Regulation (EU) 2020/2094.

Data Availability Statement: The original contributions presented in this study are included in the article. Further inquiries can be directed to the corresponding author.

Conflicts of Interest: M.C. and I.A. were employed by Arcelor Mittal R&D Centre. The remaining authors declare that the research was conducted in the absence of any commercial or financial relationships that could be construed as a potential conflict of interest.

Abbreviations

The following abbreviations are used in this manuscript:

ASU	Air separation unit
BARA	Bar absolute
BFG	Blast furnace gas
BOF	Basic oxygen furnace
CASOH	Calcium-assisted steel-mill off-gas hydrogen
CaL	Calcium looping
CCS	Carbon capture storage
CLC	Chemical looping combustion
DRI	Direct reduction iron
EAF	Electric arc furnace
EOR	Enhanced oil recovery
GHG	Greenhouse gas
IPCC	Intergovernmental Panel on Climate Change
LHV	Lower heating value
MEA	Monoethanolamine
NG	Natural gas
PFD	Process flow diagram
TRL	Technology readiness level
WGS	Water-gas shift

References

1. *World Steel in Figures 2024*; World Steel Association: Brussels, Belgium, 2024.
2. De Carvalho, A.; Nakamizu, M. Latest Developments in Steelmaking Capacity and Outlook Until 2026. Organisation for Economic Co-operation and Development Report. 2014. Available online: [https://one.oecd.org/document/DSTI/SC\(2024\)3/FINAL/en/pdf](https://one.oecd.org/document/DSTI/SC(2024)3/FINAL/en/pdf) (accessed on 30 December 2024).
3. Worldsteel. Climate Change and the Production of Iron and Steel. 2021. Available online: <https://worldsteel.org/climateaction/climate-change-and-the-production-of-iron-and-steel/> (accessed on 31 October 2024).
4. *Global Status of CCS 2023 Scaling Up Through 2030*; CCS Institute Report; CCS Institute: Melbourne, Australia, 2023.
5. Ren, L.; Zhou, S.; Peng, T.; Ou, X. A review of CO₂ emissions reduction technologies and low-carbon development in the iron and steel industry focusing on China. *Renew. Sustain. Energy Rev.* **2021**, *143*, 110846. [CrossRef]
6. Flores-Granobles, M.; Saeys, M. Minimizing CO₂ emissions with renewable energy: A comparative study of emerging technologies in the steel industry. *Energy Environ. Sci.* **2020**, *13*, 1923. [CrossRef]
7. Nicholas, S.; Basirat, S. Carbon Capture for Steel. Institute for Energy Economics and Financial Analysis. 2024. Available online: <https://ieefa.org/sites/default/files/2024-04/Carbon%20capture%20for%20steel-April24.pdf> (accessed on 30 December 2024).
8. ZEP. *CCS for Industry: Modelling the Lowest-Cost Route to Decarbonizing Europe*; ZEP: Brussels, Belgium, 2015.

9. Ho, M.T.; Bustamante, A.; Wiley, D.E. Comparison of CO₂ capture economics for iron and steel mills. *Int. J. Greenh. Gas Control* **2013**, *19*, 145–159. [[CrossRef](#)]
10. Griffin, P.W.; Hammond, G.P. Industrial energy use and carbon emissions reduction in the iron and steel sector: A UK perspective. *Appl. Energy* **2019**, *249*, 109–125. [[CrossRef](#)]
11. Perpiñan, J.; Peña, B.; Bailera, M.; Eveloy, V.; Kannan, P.; Raj, A.; Lisbona, P.; Romeo, L.M. Integration of carbon capture technologies in blast furnace based steel making: A comprehensive and systematic review. *Fuel* **2023**, *336*, 127074. [[CrossRef](#)]
12. I.E.A. *Report, Energy Technology Perspectives: Catalysing Energy Technology Transformations*; International Energy Agency: Paris, France, 2017.
13. Ji, G.; Yao, J.G.; Clough, P.T.; Diniz da Costa, J.C.; Anthony, E.J.; Fennell, P.S.; Wang, W.; Zhao, M. Enhanced Hydrogen production from thermochemical processes. *Energy Environ. Sci.* **2018**, *11*, 2647–2672. [[CrossRef](#)]
14. Martinez, I.; Fernandez, J.R.; Abanades, J.C.; Romano, M.C. Integration of a fluidised bed Ca/Cu chemical looping process in a steel mill. *Energy* **2018**, *163*, 570–584. [[CrossRef](#)]
15. Boon, J.; Cobden, P.D.; van Dijk, H.A.J.; van Sint Annaland, M. High temperature pressure swing adsorption cycle design for sorption-enhanced water-gas shift. *Chem. Eng. Sci.* **2015**, *122*, 219–231. [[CrossRef](#)]
16. Gazzani, M.; Romano, M.C.; Manzolini, G. CO₂ capture in integrated steel works by commercial-ready technologies and SEWGS process. *Int. J. Greenh. Gas Control* **2015**, *41*, 249–267. [[CrossRef](#)]
17. Sebastiani, F.; Lucking, L.; Saric, M.; James, J.; Boon, J.; van Dijk, H.A.J.; Cobden, P.D.; Pieterse, J.A.Z. Steam and Pressure Management for the Conversion of Steelworks Arising Gases to H₂ with CO₂ Capture by Stepwise Technology. *Separation* **2022**, *9*, 20. [[CrossRef](#)]
18. van Dijk, E.; Flores Granobles, M.; Perimenis, A.; Lukashuk, L.; van der Veer, S.; Masciocchi, B.; Manzolini, G.; van Zelm, R.; Bellqvist, D.; Dobree, J.; et al. INITIATE: CO₂ capture, re-use and sequestration through industrial symbiosis of the steel and ammonia/urea industries. In Proceedings of the 17th Greenhouse Gas Control Technologies Conference, Calgary, AB, Canada, 20–24 October 2024.
19. Erans, M.; Manovic, V.; Anthony, E.J. Calcium looping sorbents for CO₂ capture. *Appl. Energy* **2016**, *180*, 722. [[CrossRef](#)]
20. Antzaras, A.; Lemonidou, A.A. Recent advances on materials and processes for intensified production of blue hydrogen. *Renew. Sustain. Energy Rev.* **2022**, *155*, 111917. [[CrossRef](#)]
21. Kierzkowska, A.M.; Pacciani, R.; Müller, C.R. CaO-based CO₂ sorbents: From fundamentals to the development of new, highly effective materials. *ChemSusChem* **2013**, *6*, 1130. [[CrossRef](#)] [[PubMed](#)]
22. Arias, B.; Alvarez, Y.; Mendez, A.; Marques, P.; Finca, I.; Abanades, J.C. Pilot Testing of Calcium Looping at TRL7 with CO₂ Capture Efficiencies toward 99%. *Energy Fuels* **2024**, *38*, 14757. [[CrossRef](#)] [[PubMed](#)]
23. Boon, J. Sorption-enhanced reactions as enablers for CO₂ capture and utilisation. *Curr. Opin. Chem. Eng.* **2023**, *40*, 100919. [[CrossRef](#)]
24. Adanez, J.; Abad, A.; Garcia-Labiano, F.; Gayan, P.; de Diego, L.F. Progress in chemical-looping combustion and reforming technologies. *Prog. Energy Combust. Sci.* **2012**, *38*, 215–282. [[CrossRef](#)]
25. Lyngfelt, A. Chemical looping combustion: Status and development challenges. *Energy Fuels* **2020**, *34*, 9077. [[CrossRef](#)]
26. Antzara, A.; Herecleous, E.; Bukur, D.B.; Lemonidou, A.A. Thermodynamic analysis of hydrogen production via chemical looping steam methane reforming coupled with in situ CO₂ capture. *Int. J. Greenh. Gas Con.* **2015**, *32*, 115. [[CrossRef](#)]
27. Tian, S.; Li, K.; Jiang, J.; Chen, X.; Yan, F. CO₂ abatement from the iron and steel industry using a combined Ca-Fe chemical loop. *Appl. Energy* **2016**, *170*, 345–352. [[CrossRef](#)]
28. Adanez, J.; Abad, A.; Mendiara, T.; Gayan, P.; de Diego, L.F.; Garcia-Labiano, F. Chemical looping combustion of solid fuels. *Progress Energy Combust. Sci.* **2018**, *65*, 6–66. [[CrossRef](#)]
29. Martínez, I.; Fernández, J.R.; Martini, M.; Gallucci, F.; van Sint Annaland, M.; Romano, M.C.; Abanades, J.C. Recent progress of the Ca-Cu looping technology for decarbonisation of power plants and carbon intensive industries. *Int. J. Greenh. Gas Con.* **2019**, *85*, 71. [[CrossRef](#)]
30. Fernández, J.R.; Spallina, V.S.; Abanades, J.C. Advanced packed-bed Ca-Cu looping process for the CO₂ capture from steel mill off-gases. *Front. Energy Res.* **2020**, *8*, 146. [[CrossRef](#)]
31. Abbas, S.Z.; Fernandez, J.R.; Amieiro, A.; Rastogi, M.; Brandt, J.; Spallina, V. Lab-scale experimental demonstration of Ca-Cu chemical looping for hydrogen production and in-situ CO₂ capture from a steel-mill. *Fuel Process. Technol.* **2023**, *237*, 107475. [[CrossRef](#)]
32. Grasa, G.; Diaz, M.; Fernandez, J.R.; Amieiro, A.; Brandt, J.; Abanades, J.C. Blast Furnace Gas decarbonisation through Calcium assisted Steel-mill Off-gas Hydrogen production. Experimental and modelling approach. *Chem. Eng. Res. Des.* **2023**, *191*, 507–522. [[CrossRef](#)]
33. C4U Project. Available online: <https://c4u-project.eu/> (accessed on 30 December 2024).

34. Ujisawa, Y.; Tonomura, S.; Ishiwata, N.; Nabeshima, Y.; Saito, K. Topic: CO₂ breakthrough program by COURSE50 in Japanese steel industry sector. In *Energy Technology Roadmaps of Japan: Future Energy Systems Based on Feasible Technologies Beyond 2030*; Springer: Berlin/Heidelberg, Germany, 2016.
35. Kim, H.; Lee, J.; Lee, S.; Lee, I.B.; Park, J.H.; Han, J. Economic process design for separation of CO₂ from the off-gas in ironmaking and steelmaking plants. *Energy* **2015**, *88*, 756–764. [[CrossRef](#)]
36. Ramírez-Santos, A.A.; Bozorg, M.; Addis, B.; Piccialli, V.; Castel, C.; Favre, E. Optimization of multistage membrane gas separation processes. Example of application to CO₂ capture from blast furnace gas. *J. Memb. Sci.* **2018**, *566*, 324–334. [[CrossRef](#)]

Disclaimer/Publisher’s Note: The statements, opinions and data contained in all publications are solely those of the individual author(s) and contributor(s) and not of MDPI and/or the editor(s). MDPI and/or the editor(s) disclaim responsibility for any injury to people or property resulting from any ideas, methods, instructions or products referred to in the content.